

## RESEARCH LETTER

10.1002/2017GL073802

## Key Points:

- Uncertainty in simulated ozone is dominated by a few key reactions in both biomass burning and anthropogenic pollution plumes
- Uncertainty in PAN decomposition is key to controlling model ensemble spread in ozone change in biomass burning air masses
- Increased uncertainty at low temperatures results in a large increase in ensemble ozone spread, particularly from the  $\text{NO} + \text{O}_3$  reaction

## Supporting Information:

- Supporting Information S1

## Correspondence to:

S. R. Arnold,  
s.arnold@leeds.ac.uk

## Citation:

Ridley, D. A., M. Cain, J. Methven, and S. R. Arnold (2017), Sensitivity of tropospheric ozone to chemical kinetic uncertainties in air masses influenced by anthropogenic and biomass burning emissions, *Geophys. Res. Lett.*, 44, doi:10.1002/2017GL073802.

Received 12 APR 2017

Accepted 30 MAY 2017

Accepted article online 2 JUN 2017

# Sensitivity of tropospheric ozone to chemical kinetic uncertainties in air masses influenced by anthropogenic and biomass burning emissions

D. A. Ridley<sup>1,2</sup> , M. Cain<sup>3</sup> , J. Methven<sup>4</sup> , and S. R. Arnold<sup>1</sup> 
<sup>1</sup>Institute for Climate and Atmospheric Science, School of Earth and Environment, University of Leeds, Leeds, UK, <sup>2</sup>Now at Department of Civil and Environmental Engineering, Massachusetts Institute of Technology, Cambridge, Massachusetts, USA, <sup>3</sup>Centre for Atmospheric Science, Department of Chemistry, University of Cambridge, Cambridge, UK, <sup>4</sup>Department of Meteorology, University of Reading, Reading, UK

**Abstract** We use a Lagrangian chemical transport model with a Monte Carlo approach to determine impacts of kinetic rate uncertainties on simulated concentrations of ozone,  $\text{NO}_y$  and OH in a high-altitude biomass burning plume and a low-level industrial pollution plume undergoing long-range transport. Uncertainties in kinetic rate constants yield 10–12 ppbv (5th to 95th percentile) uncertainty in the ozone concentration, dominated by reactions that cycle NO and  $\text{NO}_2$ , control  $\text{NO}_x$  conversion to  $\text{NO}_y$  reservoir species, and key reactions contributing to  $\text{O}_3$  loss ( $\text{O}(^1\text{D}) + \text{H}_2\text{O}$ ,  $\text{HO}_2 + \text{O}_3$ ). Our results imply that better understanding of the peroxyacetylnitrate (PAN) thermal decomposition constant is key to predicting large-scale  $\text{O}_3$  production from fire emissions and uncertainty in the reaction of  $\text{NO} + \text{O}_3$  at low temperatures is particularly important for both the anthropogenic and biomass burning plumes. The highlighted reactions serve as a useful template for targeting new laboratory experiments aimed at reducing uncertainties in our understanding of tropospheric  $\text{O}_3$  photochemistry.

**Plain Language Summary** Computer models used to assess and predict how air pollution changes in response to emissions, and how it affects climate and human health, rely on information from laboratory experiments to prescribe the rates at which different atmospheric chemical species react. This laboratory information has uncertainties associated with experimental limitations or constraints. We show how these uncertainties affect confidence in model predictions of tropospheric ozone in two pollution plumes. Ozone is a key air pollutant, harmful to human health and vegetation, as well as a climate warming agent. We identify key reactions that lead to large uncertainty in simulated ozone and demonstrate the importance of low confidence in some reactions at low temperatures in driving large portion of ozone uncertainty. Our work serves as a key basis from which to motivate future lab experiments aimed at reducing uncertainty in our understanding of tropospheric ozone.

## 1. Introduction

Atmospheric chemistry processes control the distribution and abundance of trace constituents that affect both climate and air quality. Tropospheric ozone ( $\text{O}_3$ ) is a greenhouse gas and air pollutant, harmful to human health [e.g., Levy *et al.*, 2001; Ito *et al.*, 2005] and detrimental to vegetation and crops [Sitch *et al.*, 2007; Van Dingenen *et al.*, 2009; Hollaway *et al.*, 2012]. Ozone is produced in situ in the troposphere by photochemical oxidation of volatile organic compounds (VOCs) in the presence of nitrogen oxides ( $\text{NO}_x = \text{NO} + \text{NO}_2$ ). Globally, photolysis of  $\text{O}_3$  is the chief source of the OH radical [Logan *et al.*, 1981; Lelieveld *et al.*, 2002], controlling the lifetime of the greenhouse gas methane [Myhre *et al.*, 2013], and oxidation of gas-phase aerosol precursors [Kroll and Seinfeld, 2008]. Once exported to the free troposphere where it has a lifetime of several weeks,  $\text{O}_3$  can undergo long-range transport between continents [Jacob *et al.*, 1999; Jaffe *et al.*, 2003; Stohl *et al.*, 2003; Price *et al.*, 2004]. A robust understanding of  $\text{O}_3$  photochemistry during continental export is central to our ability to predict response of the large-scale distribution of tropospheric ozone and OH to changes in continental emissions of  $\text{NO}_x$  and VOCs, and to our estimates of contributions from long-range transport of  $\text{O}_3$  and precursors to surface  $\text{O}_3$  in a given region. Aggressive emissions reductions in Europe and the U.S. have resulted in a decrease in the frequency of peak  $\text{O}_3$  levels since the 1990s [Lin *et al.*, 2001; Soldberg and Lindskog, 2005]. However, overall emissions of  $\text{O}_3$  precursors in the Northern

©2017. The Authors.

This is an open access article under the terms of the Creative Commons Attribution License, which permits use, distribution and reproduction in any medium, provided the original work is properly cited.

Hemisphere (NH) are expected to continue to rise as economies in South and East Asia grow rapidly [Zhang *et al.*, 2009]. This is likely to lead to an increasing relative sensitivity of air quality in the western U.S. and Europe to O<sub>3</sub> formed upstream and imported during long-range transport events [Parrish *et al.*, 2009; Verstraeten *et al.*, 2015].

Models of atmospheric chemistry underpin our predictions of responses of climate and air quality to changes in anthropogenic and natural emissions. Model photochemical processes rely on data from laboratory experiments to parameterize the kinetics of chemical reactions, which are generally recommended by expert panels, based on the latest and best available laboratory data from the literature (the NASA Jet Propulsion Laboratory (JPL) [Burkholder *et al.*, 2015] and the International Union of Pure and Applied Chemistry (IUPAC) [Atkinson *et al.*, 2004; Crowley *et al.*, 2010] recommendations). The data from lab experiments used in such recommendations have uncertainties associated with experimental constraints and specific aspects of a given reaction system. Routinely, information regarding uncertainties in these parameters is not considered in model predictions; however, their impacts could potentially lead to uncertainties in simulation of key species concentrations important for climate and air quality. Here we focus specifically on the impact of kinetic data uncertainties in reactions of gas-phase HO<sub>y</sub>, NO<sub>y</sub>, and organic species on O<sub>3</sub> photochemistry in polluted plumes undergoing long-range transport. We use a Lagrangian chemical transport model and Monte Carlo ensemble approach to simulate photochemistry in two contrasting anthropogenic and biomass burning plumes. We quantify sensitivity of simulated concentrations of O<sub>3</sub> and key precursors to model kinetic parameter uncertainties using aircraft observations to provide model initialization and an observational comparison with model ensemble spread. We partition simulated uncertainty between specific reaction rates and identify key kinetic parameters that dominate the uncertainty in simulated oxidant photochemistry in the plumes and compare this uncertainty with that due to physical processes.

## 2. Methodology

### 2.1. Plume Cases and Modeling Framework

We examine two plume case studies, based on air masses sampled sequentially on multiple occasions by aircraft during the ICARTT (International Consortium for Atmospheric Research on Transport and Transformation) campaign in summer 2004 [Fehsenfeld *et al.*, 2006]. This pseudo-Lagrangian observation framework allows monitoring of air mass chemical evolution over several days [Methven *et al.*, 2006]. We use the CiTTYCAT Lagrangian chemistry model [Evans *et al.*, 2000; Pugh *et al.*, 2012; Arnold *et al.*, 2015], which includes inorganic NO<sub>x</sub>, O<sub>x</sub>, and HO<sub>x</sub> chemistry, along with a treatment of methane and NMHC oxidation and comprises 90 species and 220 reactions (see supporting information for more details) to simulate tropospheric chemistry between aircraft observation points, and the sensitivity of this chemistry to kinetic parameter uncertainties. Air mass trajectories for the ICARTT Lagrangian Cases 2 and 3 [Methven *et al.*, 2006] are calculated using the ROTRAJ (Reading Offline Trajectory) Lagrangian transport model [Methven *et al.*, 2003] and initialized with species concentrations observed within the matching time windows of Cain *et al.* [2012]. We label Lagrangian Case 2 as “biomass burning upper troposphere (BBU)” and Case 3 as “anthropogenic pollution low level (APL)”. A similar Lagrangian model framework was found to capture observed changes in O<sub>3</sub> and precursors in the same BBU case [Real *et al.*, 2007] and APL case [Real *et al.*, 2008]. Cain *et al.* [2012] used a CiTTYCAT model ensemble trajectory framework to examine the sensitivity of photochemical evolution to the representation of physical processes in these cases. Here the focus is on quantifying parametric model uncertainty associated with photochemical rates.

### 2.2. Perturbed Ensemble Methodology

The CiTTYCAT model framework has been modified to allow Monte Carlo ensemble simulations of each plume case, where each ensemble member considers a unique systematic perturbation of kinetic rate parameters in the model, per temperature-dependent parameter uncertainty estimates from the literature. Model rate constants and their uncertainties are taken from the JPL [Burkholder *et al.*, 2015] and IUPAC [Atkinson *et al.*, 2004; Crowley *et al.*, 2010] gas kinetic data recommendations and are used to set up a probability space that can be sampled by running the model with combinations of perturbed rate constants. The Latin hypercube (LHC) method [Mckay *et al.*, 2000] is used to efficiently sample the parameter space and to define ensemble perturbations. Since computational limitations prevent simulation of combinations of perturbations across the whole parameter space of 261 reaction rate constants, we first perform a set of

simulations probing the one-at-a-time effect of each reaction rate constant uncertainty on  $O_3$  and OH evolution in the plumes. From these we identify a smaller set of 73 rate constant uncertainties that have largest impacts on  $O_3$  and OH, for a full Monte Carlo simulation framework, allowing us to account for interdependencies between uncertainties in the reaction rate constants. A 2500-member ensemble was found to be sufficient to produce robust estimates of plume concentration uncertainty (see supporting information for details).

For a given reaction, the reaction rate constant,  $k$ , is commonly given by

$$k(T) = k_0 e^{-\frac{\Delta E}{RT}} \quad (1)$$

where  $k_0$  is the prefactor,  $\Delta E$  is the activation energy,  $T$  is the temperature, and  $R$  is the universal gas constant. The uncertainties in reaction rate constants are documented in the IUPAC and JPL recommendations, along with their temperature dependence. We use IUPAC recommendations for those rate constants that are not available in the JPL documentation.

The uncertainty of the rate constant increases as the temperature diverges from 298 K. The uncertainty on a given rate constant,  $f(T)$ , is calculated using the formula provided by JPL data sheets:

$$f(T) = f(298 \text{ K}) \exp \left[ g \left( \frac{1}{T} - \frac{1}{298} \right) \right] \quad (2)$$

where  $f(298 \text{ K})$  is the uncertainty factor at 298 K and  $g$  is an uncertainty parameter, both provided in the data sheets. The  $1\sigma$  uncertainty at a temperature,  $T$ , is obtained by multiplying the rate,  $k(T)$ , by the uncertainty factor,  $f(T)$ . If the reaction rate is unavailable in the JPL data sheets, we use IUPAC and the following reaction rate uncertainty formula from Atkinson *et al.* [2004]:

$$\Delta \log k(T) = \Delta \log k(298 \text{ K}) + 0.4343 \left\{ \frac{\Delta E}{R} \left( \frac{1}{T} - \frac{1}{298} \right) \right\} \quad (3)$$

where  $\Delta \log k(T)$  is the  $2\sigma$  uncertainty of the reaction rate constant at temperature,  $T$ . In both cases, the uncertainty as a function of temperature is not determined by rigorous statistical analysis, but through subjective assessment by evaluators.

The model ensembles are run both with and without temperature dependence of the rate constant uncertainties included in equations (2) and (3). Comparing these two sets of ensembles gives information on the uncertainty in plume chemistry introduced by the poorer knowledge of kinetic parameters at temperatures farther from 298 K. For further details of the ensemble simulation method see supporting information.

We determine the reaction rates that produce the majority of the uncertainty in simulated  $O_3$  using a multiple linear regression for each of the reaction rates as a function of the simulated perturbation to the  $O_3$  concentration. As meteorological and chemical conditions change over the duration of plume transport, the effect of rate constant uncertainties is assessed after 2, 3, and 6 days of trajectory transport to evaluate the time dependence of the uncertainty in simulated  $O_3$ .

### 3. Results

#### 3.1. Evolution of Ozone Uncertainty

Figures 1 and 2 show the time evolution of  $O_3$ ,  $NO_y$ , CO, and OH in the simulated APL (anthropogenic pollution low-level) and BBU (biomass burning upper troposphere) air masses, respectively. The plotted envelopes display the 5th, 25th, 75th, and 95th percentile concentrations based on 2500 model simulations. The range of aircraft observations from downstream interception of the air masses are shown as vertical bars, representing one standard deviation on either side of the mean observed concentrations in each Lagrangian match window [Cain *et al.*, 2012].

The spread of  $O_3$  concentrations produced by the kinetic uncertainties in the APL case (Figure 1a) increases rapidly after around 0.7 days, at the onset of daylight. Peroxyacetylnitrate (PAN) shows the largest fractional spread of the  $NO_y$  species, partly reflecting the spread in its precursor  $NO_2$ , as well as uncertainties in the specific rate of its formation (see section 3.3.1). Large spread in the nighttime  $NO_y$  reservoir species  $N_2O_5$  partly results from ensemble spread in its precursor species (including production of  $NO_3$ , which is impacted by ensemble spread in both  $NO_2$  and  $O_3$ ). Spread in  $N_2O_5$  appears to be a key driver of spread in daytime  $NO_x$ , due to the reformation of  $NO_2$  from  $N_2O_5$  at sunrise. This reformation of  $NO_2$  is limited by heterogeneous

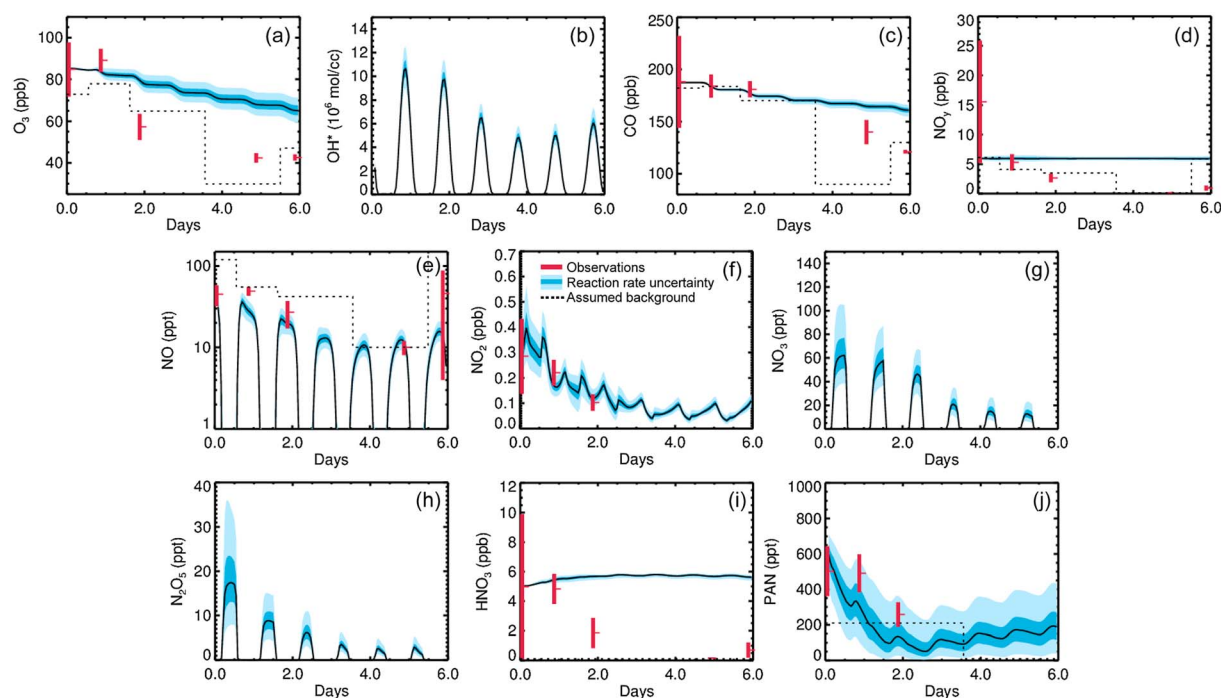


**Figure 1.** Time evolution of simulated ozone, OH, CO, and  $\text{NO}_y$  concentrations in the APL air mass, with uncertainty ranges based on 10 Monte Carlo model ensembles, each comprising 500 perturbed rate simulations. Median ensemble concentrations are shown in black. Dark blue and light blue shading show 25th to 75th percentile and 5th to 95th percentile ranges, respectively. Red vertical bars and symbol show observed standard deviation and mean concentrations observed by ICARTT campaign aircraft within the air mass [Real et al., 2007, 2008]. Black dashed lines indicate the background concentration assumed in the model, based on ICARTT observations [Real et al., 2007, 2008]. Note that simulated air mass dilution with background air and surface deposition mean that total  $\text{NO}_y$  is not conserved.

conversion of  $\text{N}_2\text{O}_5$  to nitric acid ( $\text{HNO}_3$ ) overnight.  $\text{O}_3$  spread increases to 5.6 ppbv (from the 5th to 95th percentile) by the end of the first 24 h and continues to increase throughout the simulation, reaching 9.6 ppbv after 3 days, and a maximum of 11.9 ppbv at the end of the 6 day simulation.  $\text{NO}_2$  concentrations and their spread decrease after day 3, as concentrations of  $\text{NO}_2$  reservoir species (PAN and  $\text{N}_2\text{O}_5$ ) reduce substantially. Although ensemble spread in OH (Figure 2b) does contribute to spread in CO (Figure 2c), the effect is small (11.1 ppbv) due to the long CO lifetime (approximately 90 days in this air mass). CO loss is dominated by plume dilution with surrounding background air. We assume a piecewise constant background concentration based on the observations [Real et al., 2008]. Impacts of mixing assumptions on simulated air mass chemistry are discussed in section 3.2.

Ensemble spread in  $\text{O}_3$  is initially small in the BBU case (Figure 2a) and begins to expand after around 2.3 days to reach a maximum spread of 9.9 ppbv (from the 5th to 95th percentile) after 5.8 days. The increase in spread corresponds with the time when the air mass begins to descend in altitude, reaching warmer temperatures (see supporting information Figure S1), promoting the thermal decomposition of PAN to reform  $\text{NO}_2$ . This effect can be seen in Figures 2f and 2j, showing the time series of  $\text{NO}_2$  and PAN. The spread in  $\text{NO}_2$  and PAN increases onward from 2.3 days, reaching respective spreads of 0.14 ppbv after 3.0 days and 0.44 ppbv after 6.0 days. Ensemble spread in PAN decomposition rate is the key determinant of  $\text{O}_3$  spread in this plume, due to PAN's role as the source of  $\text{NO}_2$  for  $\text{O}_3$  production (see section 3.3.2). From the same point in time, spread in  $\text{HNO}_3$  increases, due to the increased ensemble spread in  $\text{NO}_2$  and OH. Spread in OH again produces small spread in CO (7.2 ppbv) due to its long chemical lifetime. Real et al. [2007] showed that dilution with background air dominates loss in CO in this case, as also discussed for the APL case. As in the APL case, spread in  $\text{N}_2\text{O}_5$  and  $\text{NO}_3$  are also evident in the BBU case, contributed to by the spread in  $\text{NO}_2$  and  $\text{O}_3$ . Cain et al. [2012] also showed increased sensitivity to physical parameters after the initial 2 days of simulation of the BBU case. Modeled mixing rates, in particular, impacted chemical  $\text{O}_3$  production through dilution of  $\text{O}_3$  precursor concentrations, producing  $\text{O}_3$  concentrations that were 3 up to ppbv higher (lower) with weaker (stronger) mixing.

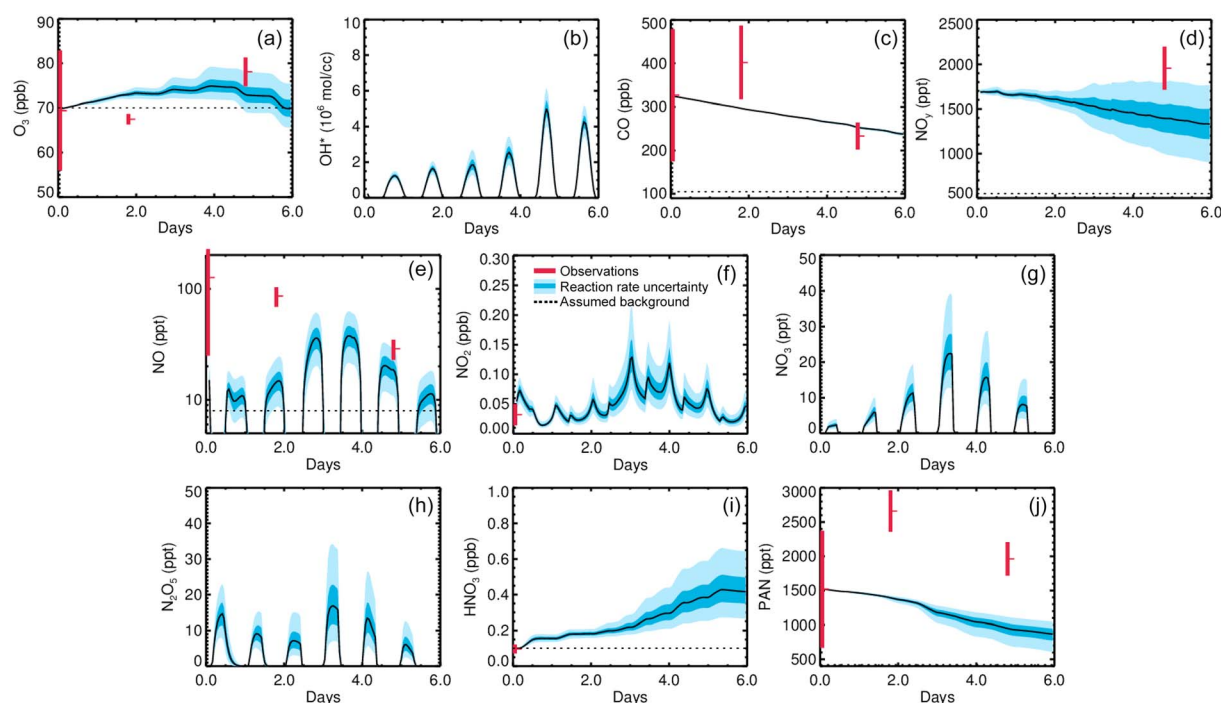


**Figure 2.** As in Figure 1 but for the BBU air mass simulations.

There is good agreement between the model and observations from the P3 and Falcon aircraft within Lagrangian match windows of NO, NO<sub>2</sub>, PAN, and CO for the APL Case (Figure 1). However, the trajectory used has a high bias in water vapor of approximately 5 g/kg, and both O<sub>3</sub> and CO do not decline as rapidly as observed along the trajectory. The model does not reproduce the observed factor of 5 decline in HNO<sub>3</sub> concentration that the observations suggest, similar to *Real et al.* [2008]. This is likely explained by a lack of dry deposition in the model trajectory; *Cain et al.* [2012] show that transition of the air mass into the boundary layer can yield rapid dry deposition of HNO<sub>3</sub>, with wet deposition playing a secondary role. For the BBU case, the model overestimates observed O<sub>3</sub> and NO, while underestimating CO and PAN. However, the model ensemble encompasses observed O<sub>3</sub>, NO, and total NO<sub>y</sub> after 4.5 days, while PAN remains underestimated (a consequence of the large uncertainty in PAN concentrations from which the model is initialized). Despite the underestimate in observed absolute PAN concentration, the upper range of simulated PAN lost to thermal decomposition (which provides a source of NO<sub>2</sub> to the air mass) during descent of the air mass is on the same order as that observed (ensemble range 270–790 pptv versus ~700 pptv observed between match windows). *Cain et al.* [2012] explored the sensitivity of CiTTyCAT model concentrations in these cases to uncertainties in initial conditions of the trajectory and found a model spread between 10 and 30 ppbv for O<sub>3</sub> in the APL case and an initial spread of 40 ppbv for the BBU case that tended toward a spread of 10 ppbv by the end of the simulation. The model sensitivity to different physical parameters and VOC chemistry produced up to a 5 ppbv and a 7 ppbv range of O<sub>3</sub> mixing ratios in the BBU case, respectively, and up to 20 ppbv for both sensitivities in the APL case. These uncertainties confound comparison with observations; however, the broad agreement with observed air mass chemical changes suggests that the key chemical processes are being captured sufficiently well to explore the sensitivity of the simulated O<sub>3</sub> to individual reaction rate kinetics.

### 3.2. Influence of Mixing

We explore the sensitivity of the simulated concentrations and spread of species resulting from kinetic uncertainties to the rate of mixing between the plume and background concentrations. For the standard APL simulation, we assume a polluted layer depth of 1500 m and use the 50th percentile mixing rate ( $\kappa_{\text{mid}} = 1.2 \text{ m}^2 \text{ s}^{-1}$ ) derived from observed changes in VOC ratios within the air mass from



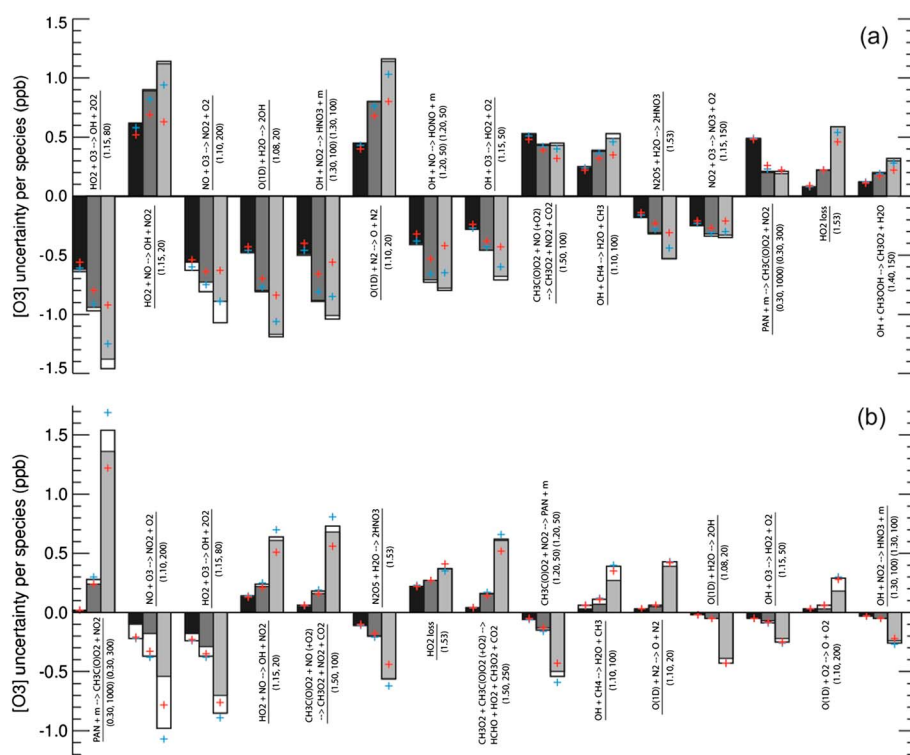


**Figure 3.** Air mass ozone uncertainty resulting from 1 sigma uncertainties in different reaction rates after 2 (black), 3 (dark grey) and 6 days (light grey), derived from Monte Carlo model ensembles comprising 2500 perturbed rate simulations for (a) the APL case and (b) the BBU case. Reactions are ordered by the average contribution to the  $O_3$  uncertainty over the 6 day period. Solid bars show ozone response based on application of reaction rate uncertainties at 298 K. Unfilled parts of each bar show the uncertainty contribution resulting from temperature dependence of the rate parameter uncertainties. The uncertainty when using the 25th and 75th percentile mixing rates are shown as the blue and red crosses, respectively. The underlined reactions appear in both cases. The reaction rate uncertainty factors,  $f(298\text{ K})$  and  $g$ , are included in brackets under the reaction for reference. There are two sets of uncertainty factors for the termolecular reactions and the 1 sigma uncertainty on the gamma factor is shown for the heterogeneous reactions. See text for details.

Arnold *et al.* [2007] and we repeat the simulations with the 25th and 75th percentile values of the mixing rate ( $\kappa_{\text{slow}} = 0.52\text{ m}^2\text{ s}^{-1}$  and  $\kappa_{\text{fast}} = 1.56\text{ m}^2\text{ s}^{-1}$ ). Both the slower and faster mixing rates cause the  $O_3$  concentration to drop more rapidly, yielding 8% and 12% less ozone after 6 days (see Figures S2 and S3). The spread in the  $O_3$  concentration owing to the reaction rate constant uncertainties is also reduced for both mixing rate limits (the spread in  $O_3$  is 8.8 ppbv for the slower mixing rate and 7.6 ppbv for the higher mixing rate after 3 days). Faster mixing reduces  $O_3$  directly through relaxation to lower background  $O_3$  concentrations. In the slower mixing case,  $NO_2$  is suppressed compared with the standard case, due to slower mixing of elevated background NO into the air parcel, as well as less mixing of PAN into the air mass at day ~3, resulting in slower photochemical  $O_3$  formation. Reduction in ozone is therefore due to physical mixing of ozone in one case, and due to chemical response to lower  $NO_x$  (due to less mixing) in the other case. Since loss of  $O_3$  is driven by first-order kinetics (i.e., it is dependent on the concentration of  $O_3$  itself), the stronger decrease in  $O_3$  over the course of the trajectory likely also limits the simulated spread in  $O_3$ . For the BBU case, mixing has less influence on the ensemble  $O_3$  simulation. The 25th, 50th, and 75th percentile mixing rates from Arnold *et al.* [2007] are  $\kappa_{\text{slow}} = 0.65\text{ m}^2\text{ s}^{-1}$ ,  $\kappa_{\text{mid}} = 0.91\text{ m}^2\text{ s}^{-1}$ , and  $\kappa_{\text{fast}} = 1.56\text{ m}^2\text{ s}^{-1}$ , respectively. In this case the  $O_3$  concentration is changed by <1% for each mixing scenario (see Figures S4 and S5). The spread in  $O_3$  is increased by 6% after 3 days for the slower mixing rate and reduced by 11% for the faster mixing rate.

### 3.3. Rate-Specific Ozone Uncertainty

The perturbation in  $O_3$  resulting from a  $1\sigma$  change in each reaction rate can be estimated by linear regression of the  $O_3$  concentration at a given time against the set of perturbed rates used. These  $O_3$

sensitivities (Figure 3) are calculated at 2, 3, and 6 days into the plume transport to show the relative importance of each rate uncertainty as chemistry evolves. Reactions are ranked based upon the average contribution to the  $O_3$  uncertainty over the 6 day simulation period. The results from the fixed-temperature ensembles are used to determine how much of the uncertainty can be attributed to temperature by taking the difference in the  $O_3$  perturbation between ensembles using uncertainties with full reaction rate temperature dependence and those simply assuming uncertainties based on 298 K. The uncertainty in  $O_3$  resulting from temperature effects is shown as the unfilled part of the bars in Figure 3. The effect of the temperature uncertainty is greater in the BBU case than in the APL case, since the ambient temperature stays closer to 298 K in the APL case (temperature, pressure, and water vapor for the simulation are displayed in Figure S1).

### 3.3.1. APL Case

For the APL case, uncertainty in  $O_3$  is dominated by uncertainty in reactions controlling  $O_3$  loss (reaction of  $HO_2 + O_3$  and loss of  $O(^1D)$  through reaction with  $H_2O$ ), and fundamental reactions governing the cycling and loss of  $NO_x$  ( $HO_2 + NO$ ;  $NO + O_3$ ;  $OH + NO_2$ ). These reactions are key in determining the net change in  $O_3$  through their controls on  $O_3$  loss and the  $NO_2$  abundance. The impact of these rate uncertainties on  $O_3$  increases by 20–40% between day 2 and day 3 and then by a similar percentage again by day 6. Uncertainty in the reaction of  $HO_2 + NO$  produces comparable, but opposite sign response in  $O_3$  to the  $HO_2 + O_3$  loss reaction uncertainty. Six day  $O_3$  responses to uncertainties in  $O(^1D) + H_2O$ ,  $NO + O_3$ , and  $OH + NO_2$  are of comparable magnitudes (1.04–1.19 ppbv), with temperature dependence of the  $NO + O_3$  uncertainty increasing the  $O_3$  uncertainty by 20%. Impact of the uncertainty in the quenching of  $O(^1D)$  to  $O(^3P)$  is comparable but opposite in sign to that in the  $O(^1D) + H_2O$  reaction, due to the importance of the competition between these reactions in controlling net  $O_3$  loss. Although we apply uncertainties in absolute rate constants for  $O(^1D)$  reactions, since these are recommended in the JPL assessment, we note that there are smaller uncertainties quoted for relative  $O(^1D)$  rate constants determined in some studies [e.g., Carl, 2005].

Uncertainties in reactions that play a role in the interconversion of PAN and its precursors are relatively more important on short timescales in the APL case. Uncertainty in PAN decomposition and in the reaction of  $MeCO_3$  with  $NO$  both contribute a positive perturbation to  $O_3$  of approximately 0.5 ppbv on a 2 day timescale; the latter being a route for cycling  $NO$  to  $NO_2$ , competing with  $NO_2$  loss via  $MeCO_3 + NO_2$ . On longer timescales, these reactions become less important in this air mass as  $NO_2$  concentrations decline and the warm, moist environment favors loss of  $NO_2$  via reaction with  $OH$  to form  $HNO_3$ . Uncertainty in this reaction contributes an  $O_3$  uncertainty of more than 1.0 ppbv after 6 days. Uncertainty in the reaction of  $OH + CH_4$  produces the same but opposite sign  $O_3$  response to the heterogeneous hydrolysis of  $N_2O_5$  (+0.53 and –0.53 ppbv respectively after 6 days), due to their respective roles in supply of peroxy radicals and loss of  $NO_x$ .

The mixing rate assumed for the air mass has no significant impact on the relative importance of reaction rates for the APL case. However, the mixing sensitivity tests show a decrease in the  $O_3$  uncertainty of up to 18% when the slower mixing rate is used and up to 47% decrease when the faster mixing rate is used.

### 3.3.2. BBU Case

Uncertainty in net  $O_3$  change in the BBU case on a 6 day timescale is dominated by the uncertainty in the PAN decomposition rate, producing an  $O_3$  sensitivity of more than 1.5 ppbv. This is the largest 1 sigma sensitivity overall in this simulated case. Increased  $O_3$  response to this rate constant uncertainty later in the transport event occurs due to descent of the air mass to warmer temperatures, promoting decomposition of PAN to release  $NO_2$ . As in the APL case, uncertainty in the reactions of  $NO + O_3$  and  $MeCO_3 + NO$  also produces a large  $O_3$  sensitivity after 6 days (0.98 and 0.73 ppbv magnitude, respectively), due to their roles in  $NO$  to  $NO_2$  cycling, and the latter's competition with PAN formation. Reaction of  $MeCO_3$  with  $CH_3O_2$  directly competes with the PAN formation reaction, and uncertainty in this reaction produces a substantial  $O_3$  response in the BBU case after 6 days (0.62 ppbv). Uncertainty in the  $HO_2 + NO$  reaction, a key route for cycling of  $NO$  to  $NO_2$ , produces a response of similar magnitude after 6 days.

After only 2 days, PAN is stable due to lower temperatures in the upper troposphere, and uncertainty in the PAN decomposition rate produces a smaller  $O_3$  uncertainty. Two day  $O_3$  response is dominated by uncertainty in reactions determining ozone loss, particularly  $NO + O_3$  and  $HO_2 + O_3$ .

The BBU case demonstrates substantial effects of increased kinetic uncertainties at lower temperatures (white bars in Figure 3b). This sensitivity is due to temperatures in the UT air mass being substantially lower than 298 K, at which kinetic parameter uncertainty is minimum [Burkholder *et al.*, 2015]. Sensitivity to the temperature dependence of the uncertainty in the rate of  $\text{NO} + \text{O}_3$  is substantial, increasing the  $\text{O}_3$  response to uncertainty in this reaction by between 45 and 55%, contributing an  $\text{O}_3$  sensitivity after 6 days of 0.44 ppbv of a total of 0.98 ppbv. The documented temperature dependence of uncertainty in this reaction is slightly larger than other key reactions (e.g., 21% at 260 K, compared with 16% for the  $\text{HO}_2 + \text{NO}$  reaction) and increases with temperature deviation from 298 K at a faster rate [Burkholder *et al.*, 2015]. Temperature effects on  $\text{O}_3$  uncertainty are also substantial for PAN decomposition and  $\text{HO}_2 + \text{O}_3$  reactions after 6 days, increasing the  $\text{O}_3$  uncertainty by 11% and 12%, respectively.

The mixing rate assumed for the air mass has no significant impact on the relative importance of reaction rates, as with the APL case. The effect of uncertainty in mixing is weaker in the BBU case, with slower mixing contributing up to a 10% increase in the  $\text{O}_3$  uncertainty and faster mixing up to a 20% decrease.

#### 4. Discussion and Conclusions

The range in simulated ozone concentrations due to kinetic uncertainties is 9.9 and 11.9 ppbv (5th to 95th percentile) for the BBU and APL cases, respectively. This is several times larger than estimates of the Asian contribution to surface  $\text{O}_3$  concentrations over the North American West Coast ( $\sim 1\text{--}4$  ppbv) [Brown-Steiner and Hess, 2011; Sudo and Akimoto, 2007] from long-range transport, and an order of magnitude larger than estimates of the annual trend in  $\text{O}_3$  in this region from increases in trans-Pacific inflow [Verstraeten *et al.*, 2015; Cooper *et al.*, 2010; Parrish *et al.*, 2009]. The range in ozone is comparable with intermodel standard deviation in present-day surface and lower tropospheric ozone concentrations among current generation global models of tropospheric chemistry [Young *et al.*, 2013].

Our results imply particularly poor constraint on our knowledge of ozone chemistry in biomass burning plumes transported to the upper troposphere. This may have important implications for simulating tropospheric oxidant chemistry in the tropical troposphere, where biomass burning emissions are rapidly transported vertically in deep convection and are an important source of ozone and precursors [Anderson *et al.*, 2016; Singh *et al.*, 2000; Folkins *et al.*, 1997]. Uncertainty in biomass burning emission impacts on upper tropospheric ozone has important implications for our confidence in radiative forcing from anthropogenic changes in tropospheric ozone [Rap *et al.*, 2015].

Uncertainty in simulated  $\text{O}_3$  in the two air masses is dominated by kinetic uncertainties in reactions that cycle NO and  $\text{NO}_2$ , reactions controlling conversion of  $\text{NO}_x$  to  $\text{NO}_y$  reservoir species, plus key reactions contributing to  $\text{O}_3$  loss ( $\text{O}(^1\text{D}) + \text{H}_2\text{O}$ ,  $\text{HO}_2 + \text{O}_3$ ). Twelve of the fifteen leading rate constant uncertainties contribute to  $\text{O}_3$  uncertainty in both the APL and BBU cases (underlined in Figure 3). The large PAN loading of the BBU case and air mass descent to warmer temperatures means that  $\text{O}_3$  production in this plume is highly sensitive to uncertainty in the rate of PAN thermal decomposition. Large PAN loadings are commonly observed in biomass burning plumes, meaning that understanding of  $\text{O}_3$  production from biomass burning emissions on a large scale may be sensitive to this rate uncertainty. Uncertainty in the rate of  $\text{O}_3 + \text{NO}$  is a key driver of  $\text{O}_3$  uncertainty in both cases, and the larger uncertainty of this reaction rate at low temperatures produces considerable uncertainty, particularly in the upper tropospheric BBU case. The reaction of  $\text{HO}_2 + \text{NO}$  ranks highly in its contribution to plume  $\text{O}_3$  uncertainty in both cases, illustrating its crucial role in determining available  $\text{NO}_2$  for  $\text{O}_3$  production.

Chemical transport models routinely use the same kinetic rate constants provided by the JPL and IUPAC assessments used here. The uncertainty in  $\text{O}_3$  that we have demonstrated may therefore represent a so-far uncharacterized error or bias across model  $\text{O}_3$  estimates. Improved confidence in the rate parameters for these fundamental reactions, and particularly their temperature dependence in the case of  $\text{NO} + \text{O}_3$ , would allow substantial reduction in  $\text{O}_3$  production rate uncertainty. Overall, our results provide a framework for targeting new laboratory experiments aimed at reducing uncertainties in our understanding of tropospheric  $\text{O}_3$  photochemistry.



## Acknowledgments

This work was supported by the UK Natural Environment Research Council (award NE/F0060X/1) and also the UK contribution to the ICARTT experiment through the NERC ITOP project NER/T/S/2002/00580. The authors acknowledge all groups involved in the ICARTT campaigns. Please see <http://www.esrl.noaa.gov/csd/ICARTT/participants/>. Model ensemble data are available from University of Leeds on request. Aircraft observations are available via campaign references cited.

## References

- Anderson, D. C., et al. (2016), A pervasive role for biomass burning in tropical high ozone/low water structures, *Nat. Commun.*, *7*, 10,267, doi:10.1038/ncomms10267.
- Arnold, S. R., et al. (2007), Statistical inference of OH concentrations and air mass dilution rates from successive observations of nonmethane hydrocarbons in single air masses, *J. Geophys. Res.*, *112*, D10S40, doi:10.1029/2006JD007594.
- Arnold, S. R., et al. (2015), Biomass burning influence on high-latitude tropospheric ozone and reactive nitrogen in summer 2008: A multi-model analysis based on POLMIP simulations, *Atmos. Chem. Phys.*, *15*, 6047–6068, doi:10.5194/acp-15-6047-2015.
- Atkinson, R., D. L. Baulch, R. A. Cox, J. N. Crowley, R. F. Hampson, R. G. Hynes, M. E. Jenkin, M. J. Rossi, and J. Troe (2004), Evaluated kinetic and photochemical data for atmospheric chemistry: Volume I - gas phase reactions of Ox, HOx, NOx and SOx species, *Atmos. Chem. Phys.*, *4*, 1461–1738, doi:10.5194/acp-4-1461-2004.
- Brown-Steiner, B., and P. Hess (2011), Asian influence on surface ozone in the United States: A comparison of chemistry, seasonality, and transport mechanisms, *J. Geophys. Res.*, *116*, D17309, doi:10.1029/2011JD015846.
- Burkholder, J. B., S. P. Sander, J. Abbatt, J. R. Barker, R. E. Huie, C. E. Kolb, M. J. Kurylo, V. L. Orkin, D. M. Wilmouth, and P. H. Wine (2015), Chemical kinetics and photochemical data for use in atmospheric studies, Evaluation No. 18, JPL Publication 15-10, Jet Propul. Lab., Pasadena, Calif. [Available at <http://jpldataeval.jpl.nasa.gov/>].
- Cain, M., J. Methven, and E. J. Highwood (2012), Quantification of chemical and physical processes influencing ozone during long-range transport using a trajectory ensemble, *Atmos. Chem. Phys.*, *12*, 7015–7039, doi:10.5194/acp-12-7015-2012.
- Carl, S. (2005), A highly sensitive method for time-resolved detection of O(<sup>1</sup>D) applied to precise determination of absolute O(<sup>1</sup>D) reaction rate constants and O(<sup>3</sup>P) yields, *Phys. Chem. Chem. Phys.*, *7*(24), 4051–4053, doi:10.1039/B513576C.
- Cooper, O. R., et al. (2010), Increasing springtime ozone mixing ratios in the free troposphere over Western North America, *Nature*, *463*, 344–348, doi:10.1038/nature08708.
- Crowley, J. N., M. Ammann, R. A. Cox, R. G. Hynes, M. E. Jenkin, A. Mellouki, M. J. Rossi, J. Troe, and T. J. Wallington (2010), Evaluated kinetic and photochemical data for atmospheric chemistry: Volume V – heterogeneous reactions on solid substrates, *Atmos. Chem. Phys.*, *10*, 9059–9223, doi:10.5194/acp-10-9059-2010.
- Evans, M. J., et al. (2000), Evaluation of a Lagrangian box model using field measurements from EASE (Eastern Atlantic Summer Experiment) 1996, *Atmos. Environ.*, *34*, 3843–3863.
- Fehsenfeld, F. C., et al. (2006), International Consortium for Atmospheric Research on Transport and Transformation (ICARTT): North America to Europe—Overview of the 2004 summer field study, *J. Geophys. Res.*, *111*, D23S01, doi:10.1029/2006JD007829.
- Folkins, I., R. Chatfield, D. Baumgardner, and M. Proffitt (1997), Biomass burning and deep convection in southeastern Asia: Results from ASHORE/MAESA, *J. Geophys. Res.*, *102*, 13,291–13,299, doi:10.1029/96JD03711.
- Hollaway, M. J., S. R. Arnold, A. J. Challinor, and L. D. Emberson (2012), Intercontinental trans-boundary contributions to ozone-induced crop yield losses in the Northern Hemisphere, *Biogeosciences*, *9*, 271–292, doi:10.5194/bg-9-271-2012.
- Itto, K., S. F. De Leon, and M. Lippmann (2005), Associations between ozone and daily mortality—Analysis and meta-analysis, *Epidemiology*, *16*, 446–457, doi:10.1097/01.ede.0000165821.90114.7f.
- Jacob, D. J., J. A. Logan, and P. P. Murti (1999), Effect of rising Asian emissions on surface ozone in the U.S., *Geophys. Res. Lett.*, *26*, 2175–2178, doi:10.1029/1999GL900450.
- Jaffe, D. A., I. McKendry, T. Anderson, and H. U. Price (2003), Six episodes of trans-Pacific transport of air pollutants, *Atmos. Environ.*, *37*, 391–404.
- Kroll, J. H., and J. H. Seinfeld (2008), Chemistry of secondary organic aerosol: Formation and evolution of low-volatility organics in the atmosphere, *Atmos. Environ.*, *42*, 3593–3624.
- Lelieveld, J., W. Peters, F. J. Dentener, and M. C. Krol (2002), Stability of tropospheric hydroxyl chemistry, *J. Geophys. Res.*, *107*(D23), 4715, doi:10.1029/2002JD002272.
- Levy, J. I., T. J. Carrothers, J. T. Tuomisto, J. K. Hammitt, and J. S. Evans (2001), Assessing the public health benefits of reduced ozone concentrations, *Environ. Health Perspect.*, *109*, 1215–1226, doi:10.1289/ehp.011091215.
- Lin, C. Y. C., D. J. Jacob, and A. M. Fiore (2001), Trends in exceedances of the ozone air quality standard in the continental United States, 1980–1998, *Atmos. Environ.*, *35*, 3217–3228.
- Logan, J. A., M. J. Prather, S. C. Wofsy, and M. B. McElroy (1981), Tropospheric chemistry: A global perspective, *J. Geophys. Res.*, *86*, 7210–7354, doi:10.1029/JC086iC08p07210.
- Mckay, M. D., R. J. Beckman, and W. J. Conover (2000), A comparison of three methods for selecting values of input variables in the analysis of output from a computer code, *Technometrics*, *42*(1), 55–61, doi:10.1080/00401706.2000.10485979.
- Methven, J., et al. (2006), Establishing Lagrangian connections between observations within air masses crossing the Atlantic during the International Consortium for Atmospheric Research on Transport and Transformation experiment, *J. Geophys. Res.*, *111*, D23S62, doi:10.1029/2006JD007540.
- Methven, J., S. R. Arnold, F. M. O'Connor, H. Barjat, K. Dewey, J. Kent, and N. Brough, (2003), Estimating photochemically produced ozone throughout a domain using flight data and a Lagrangian model, *J. Geophys. Res.*, *108*(D9), 4271, doi:10.1029/2002JD002955.
- Myhre, G., et al. (2013), Anthropogenic and natural radiative forcing, in *Climate Change 2013: The Physical Science Basis. Contribution of Working Group I to the Fifth Assessment Report of the Intergovernmental Panel on Climate Change*, pp. 674–675, edited by T. F. Stocker et al., Cambridge Univ. Press, Cambridge, U. K., and New York.
- Parrish, D. D., D. B. Millet, and A. H. Goldstein (2009), Increasing ozone in marine boundary layer inflow at the west coasts of North America and Europe, *Atmos. Chem. Phys.*, *9*, 1303–1323.
- Price, H. U., D. A. Jaffe, O. R. Cooper, and P. V. Doskey (2004), Photochemistry, ozone production, and dilution during long-range transport episodes from Eurasia to the northwest United States, *J. Geophys. Res.*, *109*, D23S13, doi:10.1029/2003JD004400.
- Pugh, T. A. M., et al. (2012), A Lagrangian model of air-mass photochemistry and mixing using a trajectory ensemble: The Cambridge Tropospheric Trajectory model of Chemistry And Transport (CITyCAT) version 4.2, *Geosci. Model Dev.*, *5*, 193–221, doi:10.5194/gmd-5-193-2012.
- Rap, A., N. A. D. Richards, P. M. Forster, S. A. Monks, S. R. Arnold, and M. P. Chipperfield (2015), Satellite constraint on the tropospheric ozone radiative effect, *Geophys. Res. Lett.*, *42*, 5074–5081, doi:10.1002/2015GL064037.
- Real, E., et al. (2007), Processes influencing ozone levels in Alaskan forest fire plumes during long-range transport over the North Atlantic, *J. Geophys. Res.*, *112*, D10S41, doi:10.1029/2006JD007576.
- Real, E., et al. (2008), Lagrangian analysis of low altitude anthropogenic plume processing across the North Atlantic, *Atmos. Chem. Phys.*, *8*(24), 7737–7754.
- Singh, H. B., et al. (2000), Biomass burning influences on the composition of the remote South Pacific troposphere: Analysis based on observations from PEM-Tropics-A, *Atmos. Environ.*, *34*, 635–644.

- Sitch, S., P. M. Cox, W. J. Collins, and C. Huntingford (2007), Indirect radiative forcing of climate change through ozone effects on the land carbon sink, *Nature*, *448*(7155), 791–794, doi:10.1038/Nature06059.
- Soldberg, S. and A. Lindskog (2005), The development of European surface ozone. Implications for a Revised Abatement Policy, EMEP/CCC-Report 1.
- Stohl, A., C. Forster, S. Eckhardt, N. Spichtinger, H. Huntrieser, J. Heland, H. Schlager, S. Wilhelm, F. Arnold, and O. Cooper (2003), A backward modeling study of intercontinental pollution transport using aircraft measurements, *J. Geophys. Res.*, *108*(D12), 4370, doi:10.1029/2002JD002862.
- Sudo, K., and H. Akimoto (2007), Global source attribution of tropospheric ozone: Long-range transport from various source regions, *J. Geophys. Res.*, *112*, D12302, doi:10.1029/2006JD007992.
- Van Dingenen, R., F. J. Dentener, F. Raes, M. C. Krol, L. Emberson, and J. Cofala (2009), The global impact of ozone on agricultural crop yields under current and future air quality legislation, *Atmos. Environ.*, *43*, 604–618, doi:10.1016/j.atmosenv.2008.10.033.
- Verstraeten, W. W., J. L. Neu, J. E. Williams, K. W. Bowman, J. R. Worden, and K. F. Boersma (2015), Rapid increases in tropospheric ozone production and export from China, *Nat. Geosci.*, *8*, 690–695, doi:10.1038/ngeo2493.
- Young, P. J., et al. (2013), Pre-industrial to end 21st century projections of tropospheric ozone from the Atmospheric Chemistry and Climate Model Intercomparison Project (ACCMIP), *Atmos. Chem. Phys.*, *13*, 2063–2090, doi:10.5194/acp-13-2063-2013.
- Zhang, Q., et al. (2009), Asian emissions in 2006 for the NASA INTEX-B mission, *Atmos. Chem. Phys.*, *9*, 5131–5153, doi:10.5194/acp-9-5131-2009.